Charge-Pairing Mechanism of Phosphorylation Effect upon Amyloid Fibrillation of Human Tau Core Peptide†

Masafumi Inoue,‡ Akiyoshi Hirata,‡ Kazuki Tainaka,‡ Takashi Morii,‡ and Takashi Konno*,§

Institute of Advanced Energy, Kyoto University, Uji, Kyoto 611-0011, Japan, and Department of Molecular Physiology and Biophysics, Faculty of Medical Sciences, University of Fukui, Matsuoka, Eiheiji, Yoshida, Fukui, 910-1193, Japan

Received June 11, 2008; Revised Manuscript Received September 4, 2008

ABSTRACT: Phosphorylation of a fibrillogenic protein, human tau, is believed to play crucial roles in the pathogenesis of Alzheimer's disease. For elucidating molecular mechanisms of the phosphorylation effect on tau fibrillation, we synthesized a peptide, $VQIVY_{310}K$ (PHF6) and its phosphorylated derivative (PHF6pY). PHF6 is a partial peptide surrounding a plausible *in vivo* phosphorylation site Tyr310 and forms amyloid-type fibrils similar to those generated by full-length tau. Fibrillation of PHF6 and PHF6pY were studied by spectroscopic and microscopic methods, and the critical concentration of the fibrillation was determined for comparing the fibril stability. The results showed that the phosphorylation strongly influenced the fibrillation propensity of PHF6 by changing its dependency on pH and ionic strength. On the basis of the observations, we suggested that charged sites on the phosphate group and its electrostatic pairing with the neighboring charged residues were physical origins of the phosphorylation effect. To verify this charge-pairing mechanism, we conducted experiments using a series of PHF6 derivatives with non-native charge distributions. The electrostatic interaction in an intermolecular mode was also demonstrated by the system composed of two different peptide species, which found that fibrillation of nonphosphorylated PHF6 was drastically enhanced when a trace amount of phosphorylated PHF6 molecules coexisted. A simulation analysis utilizing crystal coordinates of the PHF6 fibril was also performed for interpreting the experimental results in a molecular level. The present study using the model peptide system gave us a microscopically insightful view on the roles of tau phosphorylation in amyloid-related diseases.

Progressive formation of proteinaceous fibrillar inclusions in the brain, denoted as amyloid, is a hallmark pathology of human degenerative diseases. By inspecting primary sequences of many amyloidgenic polypeptides, some common features have been noticed. They found, for example, that aromatic amino acid residues, tyrosine (Tyr [1]) and phenylalanine, are key residues in generating and stabilizing the amyloid fibrils of pathogenic polypeptides (*1*), such as tau (*2*), islet amyloid polypeptide (*3*), and β-amyloid peptide (*4*). Studies focusing on the Tyr residue of amyloidgenic polypeptides are also important because it is a target of *in vivo* biochemical modifications, such as phosphorylation and oxidation, which play crucial roles in the pathogenesis of degenerative diseases (*5*−*7*). The inspections on the amyloidgenic sequences also gave hints for studies using amyloid-prone partial peptides derived from the pathogenic proteins (*2, 8*−*11*). The usage of the short peptide segments made it possible to investigate the amyloid phenomenon in atomic details. For example, recent reports utilizing microcrystals of the short amyloidgenic peptides could determine atomic structures of many amyloid species (*12*), which suggested a rational classification of the amyloid fibril structures (*13*).

Phosphorylation/dephosphorylation of human tau protein is believed to be involved in the onset of Alzheimer's disease (AD) (*14*−*17*). Hyperphosphorylated tau is the major protein component of the tangles of paired helical filaments (PHF) and straight filaments in the AD brain (*18*−*20*). Some of the phosphorylation sites at serine or threonine residues have been demonstrated to regulate binding to microtubules and fibril formation of tau (*21, 22*). Previous studies have also characterized three tyrosine residues, Tyr18, Tyr310, and Tyr394, as plausible tau phosphorylation sites in Alzheimer's PHF (*23*−*25*). Here, we focus the phosphorylation at Tyr310 because the residue is located in the microtubule-binding domain, a plausible nucleation core for the PHF formation (*26*−*28*). Modification at Tyr310 must be the most effective in altering its fibril-forming propensity and could have primary importance in biogenesis of the PHF fibrils in the AD brain.

† This work was supported in part by the Grants-in-Aid for Scientific Research from the Ministry of Education, Science, Sports and Culture, Japan to T.M. (No. 17310125 and 19021023) and to T.K. (No. 18570150 and 20570149).

* To whom correspondence should be addressed. Tel: +81-776-61-8627. Fax: +81-776-61-8101. E-mail: konno@u-fukui.ac.jp.

‡ Kyoto University.

§ University of Fukui.

[1] Abbreviations: Tyr, tyrosine; AD, Alzheimer's disease; PHF, paired helical filament; PHF6, the tau-derived VQIVYK peptide; Fmoc, 9-fluorenylmethoxycarbonyl; HBTU, 2-(1*H*-benzotriazole-1-yl)-1,1,3,3-tetramethyluronium hexafluorophosphate; HOBt, 1-hydroxybenzotriazole; DIEA, *N*,*N*-diisopropylethylamine; TFA, trifluoroacetic acid; DMF, *N*,*N*-dimethylformamide; HFIP, 1,1,1,3,3,3-hexafluoro-2-propanol; TNBS, 2,4,6-trinitrobenzenesulfonate; TMSBr, trimethylsilyl bromide; ThT, thioflavin T; TEM, transmission electron microscopy; FTIR, Fourier transform infrared; CD, circular dichroism; Lys, lysine.

10.1021/bi8010994 CCC: $40.75
Published on Web 10/16/2008

In this study, to elucidate molecular details of interplay between Tyr310 phosphorylation and tau fibrillation, we synthesized $VQIVY_{310}K$ (PHF6) derived from a partial sequence surrounding Tyr310. It has been reported that PHF6 has strong amyloid forming potential and forms fibrils with PHF-like morphology (*29, 30*). We previously found that replacement of Tyr310 of this peptide with non-natural derivatives such as 4-phenylphenylalanine or 4-methylphenylalanine drastically enhanced its amyloid-forming propensity (*31*). To investigate the molecular mechanism of the phosphorylation effect upon fibrillation, the stability of aggregates were determined for PHF6 and its derivatives including phosphorylated PHF6. The results found that an electrostatic interaction of the phosphate group with the neighboring charged residues strongly influenced the amyloid formation properties PHF6. The present study utilizing the model peptide system allowed us to resolve the mechanism in atomic details.

EXPERIMENTAL PROCEDURES

Materials. Protected 9-fluorenylmethoxycarbonyl (Fmoc) amino acids, (2-(1*H*-benzotriazole-1-yl)-1,1,3,3-tetramethyluronium hexafluorophosphate (HBTU), 1-hydroxybenzotriazole (HOBt), *N*,*N*-diisopropylethylamine (DIEA), trifluoroacetic acid (TFA), and distilled *N*,*N*-dimethylformamide (DMF) were obtained from Watanabe Chemical Industry. Fmoc-PAL-PEG resin (0.4 mmol/g) was from Applied Biosystems. HPLC grade acetonitrile (Nacalai tesque) was used for both analytical and preparative HPLC. Reagent grade water was used throughout the experiments. 1,1,1,3,3,3-Hexafluoro-2-propanol (HFIP) and sodium 2,4,6-trinitrobenzenesulfonate (TNBS) were obtained from Wako Chemicals. All other chemicals were reagent grade and used without further purification. A reversed-phase C18 column (20 × 250 mm, Ultron VX-ODS, Shinwa Chemical Industry) and a RESOURCE-RPC column (3 mL, GE Healthcare) were used for purification of peptides for preparative purpose. Analytical HPLC was carried out on a reversed-phase C18 column (4.6 × 150 mm, Ultron VX-ODS, Shinwa Chemical Industry). The products were confirmed by a MALDI-TOF mass spectrometer, Voyager DE-STR (Applied Biosystems), and an NMR spectrometer, JNM-ECP300 (JEOL).

Peptide Synthesis and Purification. All of the peptides were manually synthesized by a solid-phase peptide synthesis method (0.12−0.20 mmol scale). *N*-α-Fmoc-protected amino acids, HBTU (0.6−1.0 mmol, 5 eq.), HOBt (0.6−1.0 mmol, 5 eq.), and diisopropylethylamine (1.2−2.0 mmol, 10 eq.), were used for coupling of protected amino acids. The peptide was cleaved from the resin and deprotected by A, 90%TFA-H_2O, or B, trimethylsilyl bromide (TMSBr) (1.35 mL), thioanisol (1.2 mL), 1,2-ethanditiol (0.6 mL), *m*-cresol (0.2 mL), and TFA (7.48 mL), depending on the nature of protecting groups. Deprotections of peptides prepared by using Fmoc-Tyr$(PO(NMe)_2)_2$-OH were carried out according to a protocol supplied by Novabiochem. The solution was diluted by an addition of diethyl ether to precipitate crude peptides, and the crude sample was collected by centrifugation. The crude peptide was purified by reversed-phase HPLC. HPLC conditions: with a C18 column, eluent A, 0.05% TFA-water; eluent B, 0.05% TFA-50% CH_3CN; flow rate; 5 mL/min; or with a RESOURCE-RPC column, eluent A, 50 mM $AcONH_4$−water (pH 8.0); eluent B, 50 mM $AcONH_4$ (pH 8.0)−50% CH_3CN; flow rate; 3 mL/min. The purity of peptides was confirmed by analytical reversed-phase HPLC. The products of the peptide synthesis were characterized by MALDI-TOF MS and ^{1}H NMR.

PHF6 (Ac-VQIVYK-NH_2) TOF-Mass: MW calcd. 790.96; found 791.09. ^{1}H NMR (DMSO-d_6): δ 0.73−0.85 (*m*, 18 H), 1.04 (*m*, 1 H), 1.28 (*m*, 2 H), 1.37−1.56 (*m*, 4 H), 1.70 (*m*, 4 H), 1.87 (*s*, 3 H), 1.83−1.97 (*m*, 3 H), 2.07 (*m*, 2 H), 2.65−2.92 (*m*, 4 H), 4.09−4.28 (*m*, 5 H), 4.45 (*m*, 1 H), 6.61 (*d*, J = 8.25 Hz, 2 H), 6.76 (*s*, 1 H), 7.00 (*d*, J = 8.5 Hz, 2 H), 7.04 (*s*, 1 H), 7.15 (*s*, 1 H), 7.25 (*s*, 1 H), 7.73 (*s*, 2 H), 7.76 (*s*, 1 H), 7.78 (*s*, 1 H), 7.81 (*s*, 1 H), 7.88−8.13 (*m*, 4 H), 9.17 (*s*, 1 H).

PHF6pY (Ac-VQIVpYK-NH_2) TOF-Mass: MW calcd. 870.94; found 871.07. ^{1}H NMR (DMSO-d_6): δ 0.76−0.85 (*m*, 18 H), 1.04 (*m*, 1 H), 1.20−1.80 (*m*, 10 H), 1.87 (*s*, 3 H), 1.83−1.97 (*m*, 3 H), 2.10 (*m*, 2 H), 2.72 (*m*, 4 H), 4.15 (*m*, 5 H), 4.49 (*m*, 1 H), 6.68 (*m*, 1 H), 6.90−7.20 (*m*, 5 H), 7.50−8.10 (*m*, 8 H).

PHF6CF (Ac-VQIVF(4-CO_2H)K-NH_2) TOF-Mass: MW calcd. 818.97; found 819.35. ^{1}H NMR (DMSO-d_6): δ 0.63−0.85 (*m*, 18 H), 0.99 (*m*, 1 H), 1.28−1.73 (*m*, 9 H), 1.82−1.96 (*m*, 3 H), 1.87 (*s*, 3 H), 2.07 (*m*, 2 H), 2.74−2.90 (*m*, 3 H), 3.06−3.12 (*m*, 1 H), 4.10−4.20 (*m*, 5 H), 4.61 (*m*, 1 H), 6.77 (*s*, 1 H), 7.08 (*s*, 1 H), 7.25−7.37 (*m*, 4 H), 7.70−8.12 (*m*, 12 H).

PHF6OH (Ac-VQIVYK-OH) TOF-Mass: MW calcd. 790.95; found 792.26. ^{1}H NMR (DMSO-d_6): δ 0.73−0.87 (*m*, 18 H), 1.05 (*m*, 1H), 1.28−1.75 (*m*, 9H), 1.87 (*s*, 3 H), 1.81−1.94 (*m*, 3H) 2.07 (*m*, 2H), 2.75 (*m*, 3H), 2.89 (*m*, 1H), 4.11−4.27 (*m*, 5H), 4.49 (*m*, 1H), 6.61 (*d*, J = 8.25 Hz, 2 H), 6.76 (*s*, 1 H), 7.00 (*d*, J = 8.5 Hz, 2 H), 7.24 (*s*, 1 H), 7.67 (*s*, 2H), 7.8−8.14 (*m*, 6H), 9.14 (*s*, 1H).

PHF6E (Ac-VQIVYE-NH_2) TOF-Mass: MW calcd. 790.90; found 791.07. ^{1}H NMR (DMSO-d_6): δ 0.68−0.88 (*m*, 18 H), 1.05 (*m*, 1 H), 1.39 (*m*, 1 H), 1.87 (*s*, 3 H), 1.70−2.27 (*m*, 11 H), 2.65−2.90 (*m*, 2 H), 4.09−4.24 (*m*, 5 H), 4.44 (*m*, 1 H), 6.60 (*d*, J = 7.98 Hz, 2 H), 6.75 (*s*, 1 H), 6.99 (*d*, J = 7.95 Hz, 2 H), 7.10 (*d*, J = 17.85 Hz, 2 H), 7.24 (*s*, 1 H), 7.75−8.13 (*m*, 6 H), 9.13 (*s*, 1 H).

PHF6EpY (Ac-VQIVpYE-NH_2) TOF-Mass: MW calcd. 870.88; found 870.97. ^{1}H NMR (DMSO-d_6): δ 0.70−0.76 (*m*, 18 H), 1.07−1.29 (*m*, 3 H), 1.81 (*s*, 3 H), 1.55−2.02 (*m*, 10 H), 2.43−2.69 (*m*, 2 H), 3.85−4.19 (*m*, 5 H), 4.37 (*m*, 1 H), 6.25 (*s*, 1 H), 6.69 (*s*, 1 H), 6.92−6.95 (*m*, 4 H), 7.27 (*s*, 1 H), 7.32 (*s*, 1 H), 7.75−8.08 (*m*, 6 H).

PHF6EAmF (Ac-VQIV(4-CH_2NH_2)E-NH_2) TOF-Mass: MW calcd. 803.96; found 804.11. ^{1}H NMR (DMSO-d_6): δ 0.72−0.82 (*m*, 18 H), 1.02 (*m*, 1 H), 1.1 (*s*, 1H), 1.36 (*m*, 1H), 1.63−1.7 (*m*, 3 H), 1.83 (*s*, 3 H), 1.84−2.12 (*m*, 3 H), 2.07 (*m*, 2 H), 2.78−2.82 (*m*, 1 H), 2.94−3.0 (*m*, 1 H), 3.43 (*s*, 2 H), 4.09−4.11 (*m*, 3 H), 4.18 (*m*, 1 H), 4.48 (*m*, 1 H), 6.72 (*s*, 1 H), 7.02 (*s*, 1 H), 7.04 (*s*, 1 H), 7.21 (*s*, 1 H), 7.24−7.28 (*m*, 4 H), 7.59 (*s*, 1 H), 7.83 − 8.14 (*m*, 4H).

Abbreviations for the amino acids are E, Glu; F, Phe; I, Ile; K, Lys; Q, Gln; V, Val; Y, Tyr; pY, phosphorylated tyrosine; CF, 4-carboxyphenylalanine. AmF, 4-Aminomethylphenylalanine.

Lyophilized peptides were dissolved in HFIP (10−20 mg/mL) to avoid formation of oligomeric species in the stock solution (*30*). The peptide concentration was determined by

using the molar extinction coefficient for tyrosine (ε_{275} = 1400 M^{-1} cm^{-1}) (*32*) or by quantitation of free amino group using TNBS (*33*). The stock solution of peptide with known concentration was dispensed to a microcentrifuge tube. All of the measurements were carried out by using these samples.

Time-Course Measurements of Thioflavin T (ThT) Fluorescence Intensity of PHF6 Derivatives. The fibril formation was monitored by thioflavin T (ThT) fluorescence (*34*). The peptide stock solution was diluted with HFIP for adjusting the final peptide concentration. Six microliters of the diluted sample was dispensed to a quartz cell for the fluorescence measurement. A polymerization reaction was initiated by addition of 194 μL of 20 mM MOPS buffer (pH 7.5) or 20 mM acetate buffer (pH 4.0) containing 10 μM ThT and 0.1 M NaCl. The final concentration of HFIP was 3%. Upon dilution with the buffer, fluorescence intensities at 480 nm (excitation at 440 nm; band widths of excitation/emission = 5/10 nm) were monitored by the F4500 fluorescence spectrophotometer (HITACHI, Japan). The cell folder was kept at 25 °C by a circulating water bath.

Transmission Electron Microscopy (TEM) Analysis. Nanoscale morphology of the peptide aggregates was observed by TEM using an H-7650 electron microscope (Hitachi, Japan) operated at 80 kV and magnification of 40,000×. The samples containing the aggregates were applied to carbon grids and stained with 2% uranyl acetate. The images were recorded digitally with a CCD camera of H-7650.

Spectroscopic Measurements. Fourier transform infrared (FTIR) measurements were performed on an FT/IR-680Plus spectrometer (JASCO, Japan). The sample containing the peptide aggregates was centrifuged at 15,000 rpm for 10 min. After removal of the supernatant, the precipitated aggregates were washed with pure water. The aggregates were then spread on a calcium fluoride plate and dried up. The measurement was performed with 2 cm^{-1} resolution and accumulation of 128 scans. Circular dichroism (CD) spectra of the peptide solution were measured with a J-820 CD spectrometer (JASCO, Japan) using a 0.5-mm cell at 25 °C. Each spectrum was an average of 8 scans and was corrected with a spectrum of buffer alone but not smoothed.

Computational Methods. To aid in the interpretation of the experimental results, simple computational chemistry studies were carried out on atomic structural models of the fibrils of PHF6 and its derivatives using Insight II 2000/Discovery (Accerlys Software Inc.). On the basis of the microcrystal structure of PHF6 (PDB entry 2ON9, ref. *13*), the whole geometry of the PHF6 fibrils was constructed by stacking 20 peptide pairs along the fibril axis. The structures of PHF6pY and PHF6CF have been made by replacing tyrosine with phosphorylated tyrosine and carboxylated tyrosine, respectively. The model fibrils were solvated by a 5.0 Å layer of water molecules using the SOAK option of Insight II. Two different sets of the fibril structures were constructed. Structure 1 is the one optimized from the original geometry of the crystal structure. Structure 2 rotated a phi angle of lysine at 311 (Lys311) by 180° to make it possible to form intra- and intermolecular contacts between side chains of Tyr310 and Lys311, and then was optimized. The optimized structures were obtained by energy minimization using a combination of steepest descent and conjugate gradient algorithms. The CVFF force field was used to assign the potential of peptides and water molecules, and partial charges were assigned at neutral pH. To save the computational cost of the energy minimization, all of the peptide atoms except for those of tyrosine and lysine were fixed to their original positions, and the nonbonding energy was calculated by the cell multipole method (*35*). All the energetic terms were determined for the optimized structures 1 and 2. The model structures were illustrated by PyMOL (Delano Scientific LLC).

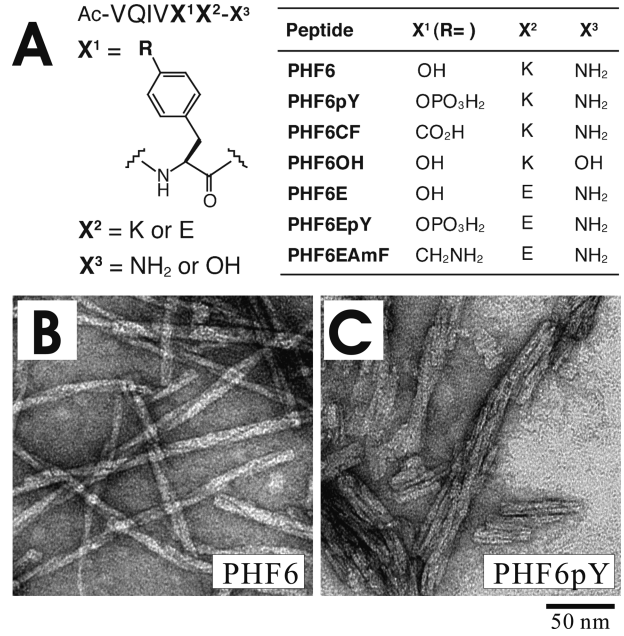

Peptide	X¹ (R=)	X²	X³
PHF6	OH	K	NH_2
PHF6pY	OPO_3H_2	K	NH_2
PHF6CF	CO_2H	K	NH_2
PHF6OH	OH	K	OH
PHF6E	OH	E	NH_2
PHF6EpY	OPO_3H_2	E	NH_2
PHF6EAmF	CH_2NH_2	E	NH_2

FIGURE 1: Structures of PHF6 derivative peptides used in this study. Chemical structures (A) and TEM images of amyloid-type fibers of PHF6 (B) and PHF6pY (C) generated by dissolving the lyophilized peptides in 20 mM MOPS (pH 7.5) and 100 mM NaCl.

RESULTS

PHF6 Derivative Peptides with Charged Aromatic Amino Acid Residues. A short peptide segment $VQIVY_{310}K$ (PHF6) corresponding to a core domain of tau is capable of forming paired-helical filaments (*2, 29*). A PHF6 derivative modified at the Tyr310 position was synthesized to generate tyrosine-phosphorylated PHF6 (PHF6pY; Figure 1A). The pK_a values of the phosphate group of phosphotyrosine are <2 and 5.8. It preserves one or two negative charges under acidic or neutral pH, respectively. A PHF6 derivative peptide having a non-natural charged amino acid residue with 4-carboxyphenyl group was also designed to elucidate electrostatic mechanisms for the phosphorylation effects (PHF6CF; Figure 1A). Other derivatives, PHF6OH, PHF6E, PHF6EpY, and PHF6EAmF, with anionic or cationic residues at the X^2 and X^3 positions were synthesized for assessing positional effects of the charged components (Figure 1).

Direct dissolution of the lyophilized peptides into an aqueous solution at neutral pH could generate peptide aggregates. TEM analysis found typical fibrillogenesis analogous to PHF formation of full-length tau. For example, PHF6 formed amyloid-type straight or paired-helical fibers (Figures 1B), whereas PHF6pY exhibited tendency to form segregated masses of the fibers (Figure 1C). Other species except for PHF6EpY could also form typical amyloid-type fibrils in the peptide concentration of 1−2 mM (Figure S1,

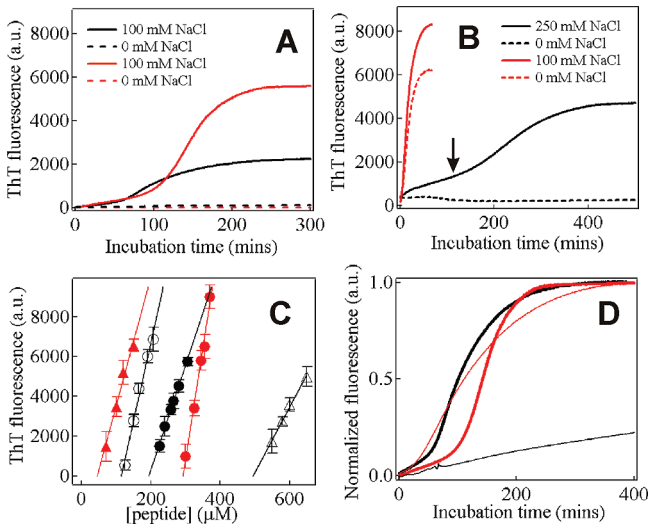

FIGURE 2: Fibrillation of PHF6 and PHF6pY monitored by changes in ThT fluorescence. All black lines and red lines indicate neutral condition (20 mM MOPS buffer, pH 7.5) and acid condition (20 mM acetate buffers, pH 4.0), respectively. All of the buffers contain 3% HFIP and 10 μM ThT. (A) The kinetic traces of PHF6 with 100 mM (solid line) or 0 mM (broken line) of NaCl. Black lines: 240 μM peptide. Red lines: 342 μM peptide. (B) The kinetic traces of PHF6pY with 250 mM (solid line) or 0 mM (broken line) of NaCl. Black lines: 720 μM peptide. Red lines: 200 μM peptide. (C) ThT fluorescence values at the final plateau phase of the kinetics data plotted against peptide concentration. Circles, PHF6; triangles, PHF6pY; black symbols, pH 7.5; red symbols, pH 4.0; filled, 100 mM NaCl; open, 250 mM NaCl. Each data point represents an average of three independent measurements. (D) Normalized kinetic traces for PHF6 (bold line) and PHF6pY (thin line) in the supersaturated concentration of 45−50 μM. NaCl concentration is 100 mM, except that the concentration for PHF6pY at pH 7.5 is 250 mM. Peptide concentrations for PHF6 are 240 μM at pH 7.5 and 342 μM at pH 4.0, and those for PHF6pY are 545 μM at pH 7.5 and 95 μM at pH 4.0.

Supporting Information). However, this experimental protocol might be inadequate for detailed analysis of the aggregation process because the lyophilized peptide samples possibly contain nuclei of the fibrillation. In the experiments below, to ensure homogeneous well-denatured peptide structures in the initial state of the aggregation, stock solutions of the peptides were made by dissolving the samples in pure HFIP, a well-known denaturant for PHF6 (*30*). Fibrillation reactions were initiated by diluting the stock solution with MOPS (pH 7.5) or acetate buffer (pH 4.0). All of the experiments below were performed in solutions containing 3% HFIP. Morphology and secondary structure content of the fibers formed in the solution containing 3% HFIP were almost the same as those in the solution without HFIP as observed by TEM and FTIR as shown below.

Aggregation Properties of PHF6 and PHF6pY. Time course of the fibril formation of PHF6 and PHF6pY was monitored by change in ThT fluorescence intensity (Figure 2A and B). The kinetic traces for PHF6 showed the initial delay phase followed by exponential increase, which is typical for nucleation-dependent amyloid type aggregation (*30, 36*). Removal of NaCl from the solution strongly suppressed the fluorescence change both at pH 7.5 and pH 4.0 (Figure 2A, broken lines). PHF6pY at pH 7.5 required higher peptide and NaCl concentrations than PHF6 for observable increase of ThT fluorescence. As an example, a black line of Figure 2B demonstrates the case of [PHF6pY] = 720 μM and [NaCl] = 250 mM. Removal of NaCl strongly inhibited the change in ThT fluorescence intensity only at pH 7.5 (Figure 2B). The typical kinetic trace of PHF6pY exhibited a two-phase change with a smaller fluorescence increase in the first phase followed by a major growth phase (Figure 2B, black line with an arrow). The aggregation kinetics of PHF6pY was faster at pH 4.0 than at pH 7.5 even at lower peptide concentrations (Figure 2B). Removal of NaCl at this pH was less effective in suppressing the aggregation (red broken line of Figure 2B).

Table 1: Apparent Critical Concentrations for Fibrillation Estimated from ThT Fluorescence Measurements[a]

species	[NaCl] (mM)	pH 7.5 (μM)	pH4.0 (μM)
PHF6	100	194 ± 2	293 ± 3
	250	115 ± 4	−[b]
PHF6pY	100	n.d.[c]	46 ± 6
	250	496 ± 6	−
PHF6CF	100	93 ± 2	63 ± 3
PHF6OH	100	350 ± 9	210 ± 3
PHF6E	100	258 ± 7	30 ± 2
PHF6EpY	100	n.d.	231 ± 2
PHF6EAmF	100	57 ± 6	157 ± 4

[a] Each value was estimated by extrapolating each plot of Figure 2C or 6 to the zero concentration axis with a linearly fitted line. Linear regression errors are also given. [b] Not measured. [c] Not determined because no significant fluorescence signal could be detected in these conditions.

For a quantitative analysis of aggregation propensity, the kinetic data were collected in several different peptide concentrations, and the fluorescence value at the final plateau phase was plotted against the peptide concentration (Figure 2C). Extrapolation of each plot to *x*-axis gave an estimate of a critical concentration (Table 1), which is a minimum peptide concentration required for yielding fibrils and could be a measure for stability of the fibril (*36, 37*). The analysis found that PHF6 had a larger tendency to form fibrils at higher pH and higher salt concentrations. In contrast, PHF6pY had much lower critical concentration at pH 4.0 than that at pH 7.5.

For comparison of the aggregation rate, the kinetic traces at the same supersaturated concentration (i.e., the bulk minus critical concentration) were normalized by the maximum ThT fluorescence value at the final plateau phase. The data in Figure 2D was thus prepared for PHF6 and PHF6pY in the neutral and acidic conditions in the supersaturated concentration of 45−50 μM. In the amyloid-type aggregation, the faster kinetic process under a fixed supersaturated concentration indicates the larger molecular association constant (*36*). The result in Figure 2D demonstrated that the aggregation rate of PHF6 in the growth phase was similar at pH 7.5 and at pH 4.0, indicating that the free energy barrier to be surmounted for the peptide association depended only marginally upon the solution pH. As for PHF6pY, however, the aggregation rate at pH 4.0 was much faster than that at pH 7.5. In this case, the data at the higher salt concentration (250 mM) was used for pH 7.5 because PHF6pY at pH 7.5 showed no observable level of aggregation in 100 mM NaCl. The result in Figure 2D also showed that the aggregation rate of PHF6pY at pH 4.0 was comparable to that of PHF6 at the same supersaturated concentration.

CD spectra of PHF6 at the final plateau phase were examined to assess its secondary structures. A single negative band between 215 and 220 nm grew during the fluorescence

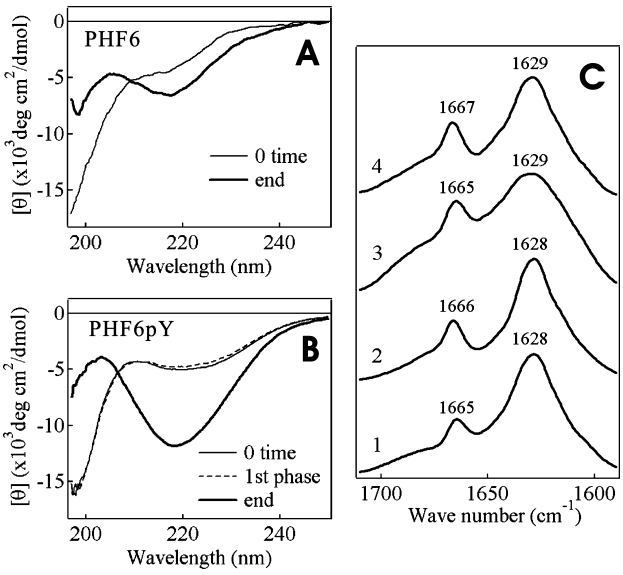

FIGURE 3: Secondary structures of PHF6 and PHF6pY. CD spectra at pH 7.5 of PHF6 (240 μM, 100 mM NaCl, panel A) and PHF6pY (720 μM, 250 mM NaCl, panel B). The spectra were taken at 0 time (thin line) and final plateau phase (thick line). A dashed line in B is the data at 2 h of incubation time. Panel C represents FT-IR bands in the amide I region characteristic of β-sheet secondary structure of PHF6 at pH 7.5 (1) and 4.0 (2), and PHF6pY at pH 7.5 (3) and pH 4.0 (4).

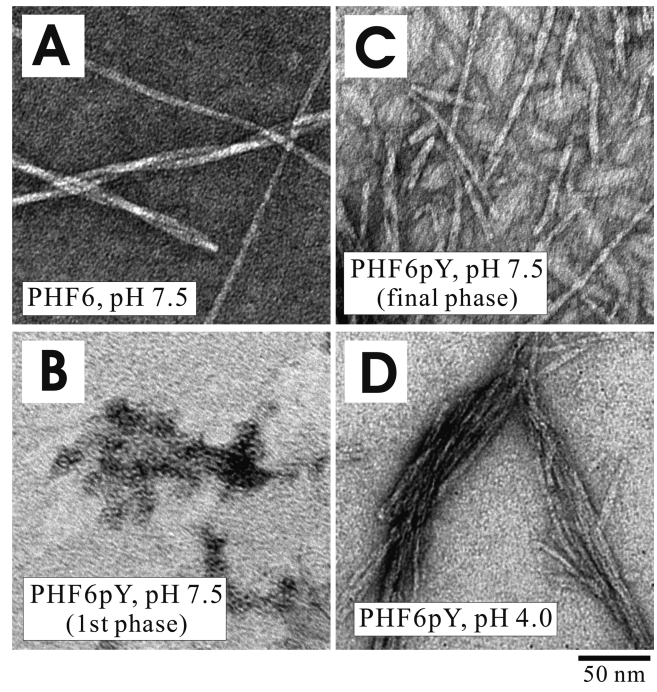

FIGURE 4: TEM images of fibrous aggregates of PHF6 and PHF6pY. The images were taken for the samples at the final plateau phase (A, C, and D) or the first phase (B; PHF6pY) of aggregation kinetics. (A) PHF6 (300 μM) at pH 7.5, 100 mM NaCl, and 2 h of incubation time. (B) PHF6pY (720 μM) at pH 7.5, 250 mM NaCl, and 2 h. (C) PHF6pY (720 μM) at pH 7.5, 250 mM NaCl, and 8 h. (D) PHF6pY (200 μM) at pH 4.0, 100 mM NaCl, and 1.5 h.

change (Figure 3A for pH 7.5), indicating that PHF6 took typical β-sheet configuration in the aggregation process. As for PHF6pY, the CD spectrum at the end of the first phase (an arrow in Figure 2B) did not show substantial change, whereas that of the final plateau stage demonstrated an evident β-sheet formation (Figure 3B), which indicated that the first phase of the fluorescence change of PHF6pY was a preparative phase preceding the formation of mature fibrils. In fact, centrifugation of the sample at the end of the first phase precipitated only a small amount of aggregates. For further secondary structural analysis, the aggregates were collected by centrifugation at the final phase of the aggregation and were subjected to FTIR measurements. The IR spectra of the PHF6 aggregates showed intense amide I bands around 1628 cm^{-1} characteristic to the β-sheet structure (Figure 3C, spectra 1 and 2) (*38*). No high frequency component between 1684 and 1704 cm^{-1} characteristic to an antiparallel strand configuration was observed, indicating that the aggregates formed by PHF6 took parallel β-sheet configuration. The IR spectral patterns for PHF6pY were the same as those of PHF6 both at pH 7.5 and 4.0 (Figure 3C, spectra 3 and 4). The CD and IR analysis showed that the secondary structure of the PHF6pY aggregates was the same as that of PHF6.

Morphological analysis of the aggregates by TEM confirmed that PHF6 formed paired helical fibers (Figure 4A at pH 7.5). The fibril properties of PHF6 revealed by TEM and spectroscopies above were similar to those of fibers formed by full-length tau (*39, 40*). The TEM analysis for PHF6pY showed that the aggregates formed at the end of the initial aggregation phase (an arrow in Figure 2B) was amorphous (Figure 4B), confirming that the first phase of PHF6pY aggregation was just a preparative one for fibrillation. The PHF6pY aggregates at the final phase demonstrated the fibrous morphology similar to those of PHF6 (Figure 4C). The PHF6pY aggregates at acidic pH represented a fibrous form with some tendency to form segregated masses of the fibers (Figure 4D).

We would emphasize here that the pH-dependency of the stability of the aggregates of PHF6pY was reverse of that of PHF6 (Figure 2C and Table 1). This could be explained by the difference in charged states of the peptides. PHF6 has a +1 charge on Lys at neutral pH, and the protonated state is more stable at acidic pH. PHF6pY carries −1 or 0 net charges in the pY-Lys site at pH 7.5 or pH 4.0, respectively. In addition, the negatively charged phosphate group is located close to Lys. For further analysis below, we postulated that the ionic states in the Tyr and Lys positions and interaction between them have strong effects on amyloid propensity of the peptide. This ionic mechanism was also supported by the relatively small effect of NaCl on the aggregation of PHF6pY at pH 4.0, where the net charge of the peptide was almost zero (Figure 2B, red broken line).

Aggregation Properties of Other PHF6 Derivatives. Aggregation properties of other PHF6-derived peptides with non-native distributions of charged residues (Figure 1A) were studied to investigate background mechanisms of the phosphorylation effect. The aggregation kinetics of all the derivatives was measured by the ThT fluorescence method (Figure 5), most of which exhibited two-phase aggregation behaviors at least in relatively low peptide concentrations. The kinetic traces in Figure 5 are those in the supersaturated concentration of ~50 μM at pH 7.5 and pH 4.0 after normalization by the maximum fluorescence value. The kinetic traces without the normalization are presented in Figure S3 (Supporting Information). The critical concentration for each case was determined from the kinetic data with various peptide concentrations (Figure 6 and Table 1). The descriptions below the results focused on the equilibrium

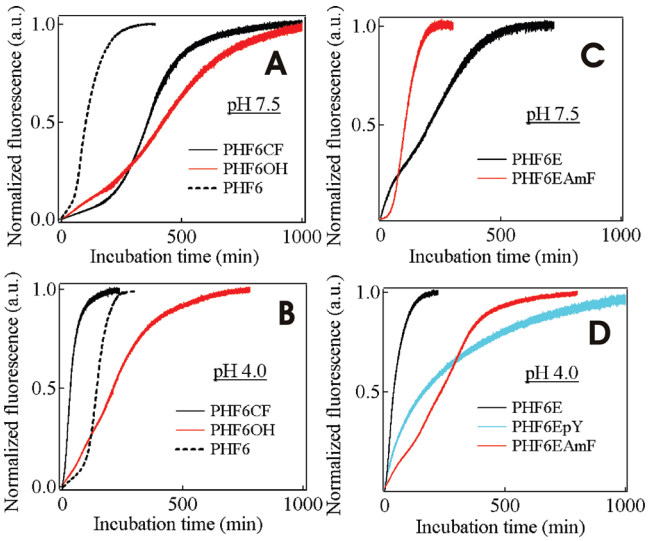

FIGURE 5: Normalized aggregation kinetics of PHF6 derivatives monitored by ThT fluorescence in the supersaturated concentration of 42−54 μM. Each trace was normalized by the maximum fluorescence value at the final plateau phase. (A) At pH 7.5 for 240 μM of PHF6 (black broken line), 150 μM of PHF6CF (black solid line) and 400 μM of PHF6OH (red line). (B) At pH 4.0 for 342 μM of PHF6 (black broken line), 111 μM of PHF6CF (black solid line), and 252 μM of PHF6OH (red line). (C) At pH 7.5 for 312 μM of PHF6E (black solid line) and 100 μM of PHF6EAmF (red solid line). (D) At pH 4.0 for 72 μM of PHF6E (black line), 198 μM of PHF6EAmF (red line), and 275 μM of PHF6EpY (blue line).

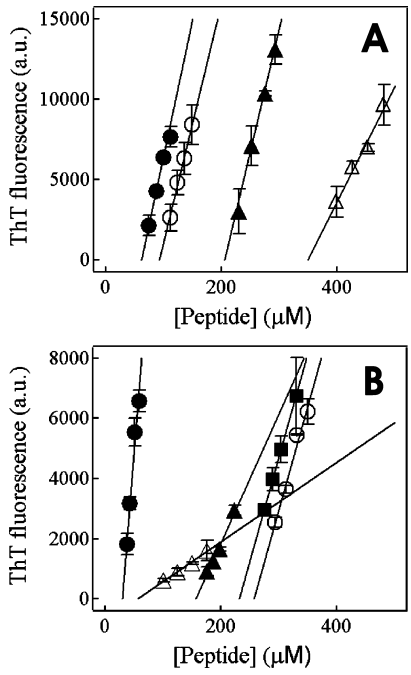

FIGURE 6: ThT fluorescence values at the final plateau phase of the kinetics data plotted against peptide concentrations. Open and filled symbols are for pH 7.5 and 4.0, respectively. (A) PHF6CF (circles) and PHF6OH (triangles). (B) PHF6E (circles), PHF6EAmF (triangles), and PHF6EpY (squares). All of the data were obtained in solutions containing 100 mM NaCl.

aspect of the aggregation assessed by the critical concentration value. This is related to the main conclusions of this article. The kinetic behaviors of the peptide association were more complicated as described later in Discussion.

The aggregation propensity of PHF6CF was examined as a test for the charge pairing between the Tyr and the Lys sites. The critical concentration for the fibrillation at pH 7.5 was smaller than that of PHF6 (Table 1). However, the critical concentration at pH 4.0 was slightly smaller than that at pH 7.5. Another derivative, PHF6OH, has a carboxylate negative charge in the C-terminal position. The critical concentration of this mutant was much higher than that of PHF6CF both at pH 7.5 and pH 4.0 (Table 1). The position of the carboxylated charged group was critical.

We also studied the cases of PHF6E and its phosphorylated derivative PHF6EpY, which have a negatively charged glutamic acid residue instead of lysine at the X^2 position (Figure 1A). The stability of the aggregates of PHF6E was smaller than that of PHF6 at pH 7.5 but larger at pH 4.0 (Table 1). The tyrosine phosphorylation of PHF6E strongly suppressed fibril formation at pH 7.5 (Figure 6B). The solution of PHF6EpY showed no substantial increase in ThT fluorescence within 24 h up to 960 μM peptide concentration. Only at pH 4.0, PHF6EpY could form aggregates (Figures 5 and 6B, and Table 1). Using the PHF6E mutant as a template, we also synthesized a charge-swapped mutant PHF6EAmF (Figure 1A), which carries a positive charge at the 310 position and a negative charge at the 311 position at neutral pH. Aggregation properties of this mutant were examined for confirmation of the charge pairing between the 310 and 311 positions. The critical concentration of the fibrillation of this mutant at pH 7.5 (Table 1) was much smaller than that of PHF6E. By reducing pH, the stability of the fibril decreased.

Figure 7 summarizes structural properties of fibrils formed by PHF6CF, PHF6OH, PHF6E, PHF6EpY, and PHF6EAmF, all of which represented the amyloid-type fibrils rich in parallel β-sheet conformation, showing that their non-native side chains did not alter the structures of the aggregates, although they strongly affected fibril stability.

Combinatorial Effects of PHF6 Derivatives. The aggregation kinetics in solutions containing two peptide species was studied to examine roles of interaction between different peptide species. First, the aggregation kinetics of the mixture of PHF6 and PHF6pY was examined at a variety of mixing ratios. The aggregation profile of pure PHF6 at 240 μM exhibited a lag phase of about 50 min and a growth phase of up to 300 min of incubation time (bold black line in Figure 8A). This profile was drastically changed by replacing only 1−2% portion of PHF6 molecules with PHF6pY. The lag time disappeared, and the aggregation rate increased (Figure 8A). The change in the aggregation kinetics profile was almost saturated at 5% of PHF6pY. The aggregates formed in the solution of PHF6+PHF6pY had TEM and IR features indistinguishable from those of pure PHF6 (Figure 8B and C).

The mixing effect with other PHF6 derivatives was studied to get insights into the background physical mechanisms. The results showed that a small amount of PHF6E or PHF6CF mixed with PHF6 drastically enhanced fibril formation (Figure 9A). The order of the efficiency was PHF6+PHF6pY > PHF6+PHF6E > PHF6+PHF6CF, which correlated well with the amount of negative charge at the Tyr-Lys (or Glu) portion of the additives. PHF6OH, which had a negative charge at the C-terminal portion, hardly affected the aggregation process of PHF6. However, the peptide mixing in the aggregation of PHF6E showed effects distinct from the case of PHF6. The order of aggregation

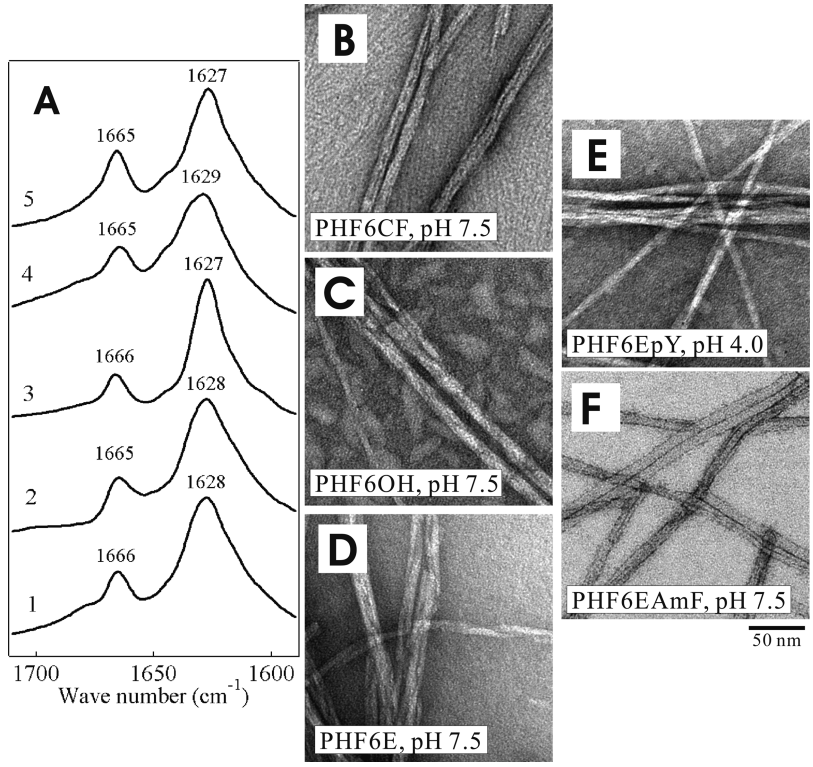

FIGURE 7: FTIR spectra and TEM images of aggregates of PHF6 derivative peptides at the final plateau phase of aggregation kinetics. PHF6CF at pH 7.5 (A-1 and B). PHF6OH at pH 7.5 (A-2 and C). PHF6E at pH 7.5 (A-3 and D). PHF6EpY at pH 4.0 (A-4 and E). PHF6EAmF at pH 7.5 (A-5 and F).

rate in this case was PHF6E+PHF6 > PHF6E+PHF6pY > PHF6E > PHF6E+PHF6EpY (Figure 9B). The aggregation tendency was decreased when the net charge value of the additive was decreased from +1 to −3.

DISCUSSION

Charge-Pairing Mechanisms of the Phosphorylation Effect. The experimental results had led us to suppose that the electrostatic nature of the phosphate group and its interaction with its surrounding residues strongly affected the amyloid-forming propensity of the tau-derived peptide PHF6. In this study, we were mainly concerned with the equilibrium aspect of the amyloid propensity of the peptides assessed by the critical concentration value and found that the stability of the aggregates correlated relatively well with the charge distribution of the peptide sequence as discussed below. However, the kinetic behaviors of the peptide association were more complicated (Figure 5). We gave only a few considerations to the kinetic aspect later.

The fibril stability of PHF6pY was much larger at pH 4.0 than at pH 7.5, whereas those of PHF6 were smaller at pH 4.0 than at pH 7.5 (Figure 2C and Table 1). For interpreting these results, we suggest that a positive charge of Lys destabilizes the peptide assembly, which can be neutralized by pairing with negative charges of phosphotyrosine at the Tyr310 site. To test the contribution of the charge of Lys to the aggregation of PHF6, we synthesized two mutant peptides VQIVYA and VQIVYS lacking any charged sites. Their aggregation showed no substantial pH dependency (Figure S2, Supporting Information), supporting that the charge on the Lys residue is one of the determinants of fibrillation and its pH-dependency of PHF6. The protonated state of Lys is more stable at acidic pH, which could elevate the free energy level of the peptide aggregates via positive electrostatic potential between closely oriented Lys residues. As for PHF6pY, two negative charges of the phosphate group at pH 7.5 can be neutralized only partially by one cationic charge of the neighboring lysine. This residual net charge could generate strong anionic repulsion in the assembled state of the peptide. In acidic conditions, however, only one anionic charge remains on the phosphate group, and the net charge of PHF6pY becomes almost zero, which could reduce the repulsive force generated at the pY-Lys portion and could stabilize the assembly of PHF6pY.

The results of PHF6E and its phosphorylated derivative PHF6EpY can be interpreted in a similar manner. The negatively charged state of Glu of PHF6E is more stable at pH 7.5 than at pH 4.0, which might explain the pH-dependency of the fibril stability of PHF6E (Figure 6B and Table 1). The phosphorylation of PHF6E introduced additional negative charges, and strong electrostatic repulsion between the PHF6EpY molecules could explain the suppression of fibrillation by phosphorylation. Fibrillation of this mutant could be observed only at pH 4.0, where the negative charges of phosphate and Glu were to be reduced (Figures 5 and 6B, and Table 1).

The essential role of the electrostatic paring between the phospho-Tyr310 and Lys311 positions was strongly confirmed by the results of the charge-swapped mutant PHF6EAmF (Figure 1A). This mutant has an amino group at the 310 position and a carboxylate group at the 311 position. The critical concentration of the mutant was much smaller than that of PHF6E at pH 7.5 (Figure 6B and Table 1), where the total charge of PHF6EAmF at the 310−311 site should be almost zero. Increase in the critical concentra-

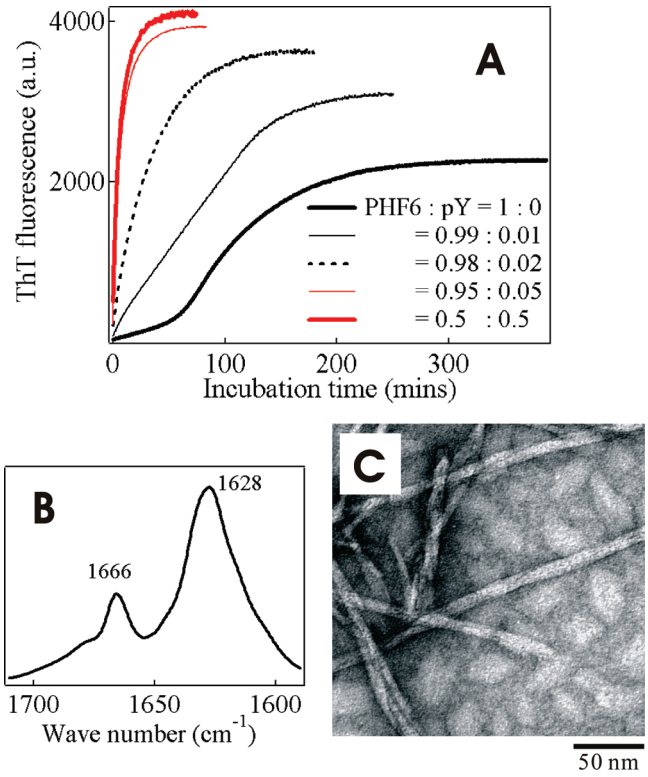

FIGURE 8: Fibrillation in solutions containing two peptide species monitored by ThT fluorescence. (A) The kinetic traces of the sample containing PHF6 and PHF6pY with a variety of the mixing ratio at pH 7.5 with 100 mM NaCl. The total peptide concentration was 240 μM. The molar ratio of [PHF6:PHF6pY] are [1.0:0.0] (bold black line), [0.99:0.01] (thin black line), [0.98:0.02] (broken black line), [0.95:0.05] (thin red line), or [0.5:0.5] (bold red line). (B and C) Structural properties of fibrils formed by 228 μM PHF6 + 12 μM PHF6pY. An IR spectrum (B) and a TEM image (C).

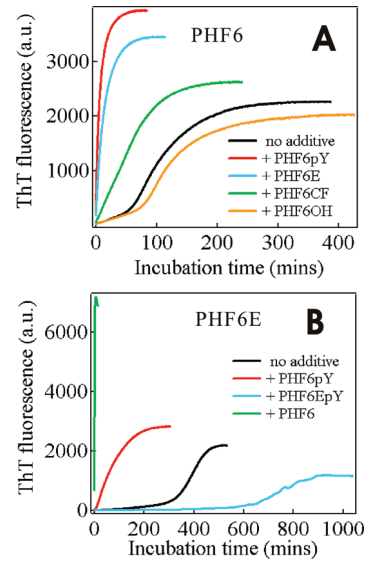

FIGURE 9: Fibrillation kinetics in solutions containing two peptide species monitored by ThT fluorescence at pH 7.5 with 100 mM NaCl. (A) The kinetic traces of the sample containing 228 μM of PHF6 + 12 μM of various PHF6 derivatives. PHF6 only (black; 240 μM PHF6), PHF6 + PHF6pY (red), PHF6 + PHF6E (blue), PHF6 + PHF6CF (green), and PHF6 + PHF6OH (orange). (B) The kinetic traces of the sample containing 270 μM of PHF6E + 30 μM of various PHF6 derivatives. PHF6E only (black; 300 μM PHF6E), PHF6E + PHF6pY (red), PHF6E + PHF6EpY (blue), PHF6E + PHF6 (green).

tion of this mutant by lowering pH could be explained by increase in the net positive charge at the 310−311 site.

The charge-paring mechanism could also explain the smaller critical concentration at pH 7.5 of PHF6CF than that of PHF6 (Figure 6A and Table 1), where a negative charge of the carboxylate group of PHF6CF could stabilize the peptide aggregates by neutralizing a positive electrostatic potential generated by Lys. The mechanism of charge pairing also implies a critical position dependency of charge-altering mutations. In fact, the negatively charged carboxylate group at the C-terminal position of PHF6OH seemed to be less effective as compared with the case of PHF6CF in counteracting with the positive charge of Lys311 (Figure 6A and Table 1).

Some of the results also indicated minor but significant deviations from the charge-pairing mechanism. For example, the critical concentration of the fibrillation of PHF6CF became smaller when the solution pH decreased (Figure 6A and Table 1), which might be unexpected because the total charge at the Tyr-Lys site should be larger at pH 4.0, and the critical concentration was therefore expected to be larger. Related to the inconsistency, we would first point out essential roles of the aromatic part of the phosphorylated Tyr. A previous report by Rojas-Quijano et al. (*30*) demonstrated very low amyloid propensity of PHF6-derived mutant peptides with negatively charged Glu or Asp residues in the place of Tyr. Removal of the aromatic part seems to reduce the amyloid propensity even when the −1 charge is on the 310 site. The Tyr phosphorylation of PHF6 we tested introduced the negative charge without removing the aromatic part of the Tyr side chain, and therefore, the charge-paring effect might be properly evaluated here. However, we should also notice that the charges on the aromatic ring could have effects other than the charge-pairing with Lys. The charges might also alter the hydrophobic or electronic atmosphere around the aromatic ring and could hinder the efficient stacking of the aromatic ring within the fibrils. This might explain at least partially the smaller critical concentration of PHF6CF at pH 4.0 than at pH 7.5 since the negative charge on the carboxylated aromatic ring should be smaller at pH 4.0. Other mechanisms could also alter the ionic state of the fibrils. For example, the pK_a values of the carboxylate, amino, or phosphate groups in the aggregates might be substantially different from those in the monomeric state because of the strong electrostatic pairing between them in the aggregates. This might affect the pH value, where the net charge of the interacting sites becomes zero.

To give some hints for the charge-pairing mechanism in molecular details, we inspected the cross-β structure of the PHF6 crystal as an atomic model of PHF6 fibrils ((*13*) PDB entry 2ON9). In the original PDB coordinates, the side chain of Lys311 faces opposite that of Tyr310 (structure 1 in Figure 10). To explain our experimental results, we were inclined to consider an alteration in the fibril structure induced by phosphorylation or carboxylation. As an example of such hypothetical structures having close contact between Tyr310 and Lys311, we propose the one obtained by a 180° rotation of the phi angle of Lys311 (structure 2 in Figure 10). A simple energetic optimization was performed for the original and the modified conformations to compare their stabilities, and we found that, for PHF6, the closer positioning of

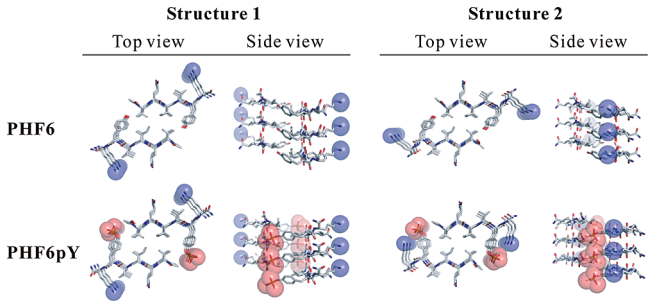

FIGURE 10: Hypothetical structures of amyloid-type fibrils formed by PHF6 and PHF6pY at neutral pH. The models represent two different types of cross β-sheet conformations of the peptide fibrils, one being optimized from original PDB coordinates (Structure 1; ref *13*, PDB entry 2ON9) and the other having a modified location of Lys311 (Structure 2). Blue: positively charged sites of Lys. Red: negatively charged sites of phosphate groups.

Lys311 to Tyr310 in the structure 2 was unfavorable by ~100 kcal/mol energetic loss caused by the molecular distortion (Figure 10 and Table S1 (Supporting Information)). However, the analysis of structure 2 of PHF6pY demonstrated strong inter/intramolecular electrostatic contacts between pY and Lys (Figure 10), and structure 2 in this case was more stable by ~100 kcal/mol than the original structure 1. The negative electrostatic term for PHF6pY was large enough to overcome the disadvantage by molecular distortion. Similar preference of structure type 2 was also found for PHF6CF. These theoretical analyses support a plausible alteration in the fibril structure induced by tyrosine phosphorylation. With minor structural changes of this kind, the cationic lysine residue might interact with the anionic phosphotyrosine of PHF6pY through inter/intramolecular electrostatic interactions.

The considerations above were concerned with the phosphorylation effect upon the stability of the fibril. The effects of peptide mutations and pH change on the association rate of the peptide were more complicated. For example, the aggregation rate of the growth phase of PHF6 at pH 4.0 was not significantly changed by phosphorylation (Figure 2D), suggesting that the electrostatic nature of the phosphate group is less critical with regard to the aggregation rate than with regard to the stability of aggregates at least in acidic conditions. The results of other derivatives also indicated a wide range of physical origins for the free energy barrier of peptide association. The aggregation rate of PHF6CF at pH 7.5 was smaller than that of PHF6, which could not be explained by the electrostatic neutralization effect, and might indicate contributions of steric or other factors (Figure 5A). The smaller aggregation rate of PHF6OH than that of PHF6 both at pH 7.5 and pH 4.0 might indicate that the negatively charged group at the C-terminal portion could generate an additional electrostatic barrier for peptide association (Figure 5). Strong decrease in the aggregation rate of PHF6E by phosphorylation, however, could be explained by the large negative charges at the pY-Glu site (Figure 5). In this study, we did not perform quantitative analysis of the kinetic data because at present we cannot propose a single mathematical function (or a kinetic model) that fits all of the kinetic data sufficiently well and consistently. Detailed studies for the kinetic process of the tau-derived peptides are now in progress.

Combinatorial Effects of Phosphorylated and Nonphosphorylated Peptides. Our results demonstrated that the aggregation propensity of PHF6pY at pH 7.5 was smaller than that of PHF6 (Table 1), which might suggest that phosphorylation of tau could reduce its fibrillogenicity. However, this view must be corrected when we consider the results for a mixture of phosphorylated and nonphosphorylated molecules (Figures 8 and 9). Interaction between the two different species could very strongly accelerate the fibrillation of the whole system. Only 1% fraction of the phosphorylated molecules clearly diminished the lag phase of the aggregation profile of PHF6, and the effect was almost saturated at the mixing fraction of 5% (Figure 8A). These results suggested that the interaction of PHF6 and PHF6pY had drastic effects primarily at the nucleation step of fibrillation. The results in Figure 9A demonstrated that the efficiency of the minor additives was proportional to the number of negative charges at the Tyr-Lys site. It is plausible that the negative charge at the phosphate group of the PHF6pY molecule makes ionic paring with ionized Lys on the neighboring PHF6 molecule (Figure 10). The strong association between the PHF6 and the PHF6pY molecules probably forms a nucleation core for fibrillation very efficiently, which could rapidly initiate the fibrillation in the heterogeneous system. These considerations have led us to propose that the effect of phosphorylation could be tremendous even when the number of phosphorylated molecules is much smaller than that of the nonphosphorylated molecules. We would also note that the interaction between the phosphorylated and the nonphosphorylated molecules does not always enhance fibril formation but may also inhibit it depending on the charge distributions of the two interacting species, which is exemplified in Figure 9B for the case of PHF6E.

Concluding Remarks. Hyperphosphorylation of tau is believed to play a crucial role in the pathogenesis of Alzheimer's disease (*5, 14*−*17*). All of the present findings support the view that tau phosphorylation can initiate or modify pathological events by influencing tau fibrillation. There exist many cationic residues in the microtubule-binding domain of tau. This domain is well known to be quite fibrillogenic when the surrounding media provide anionic circumstances (*41*−*43*). It is very likely that the phosphorylation of this critical domain affects fibril formation by interactions of the anionic phosphate group with the neighboring charged residues. The charge-pairing mechanism we proposed here indicates that phosphorylation would not always enhance fibrillogenesis but could also inhibit it. The phosphorylation effect should depend critically on the site of phosphorylation and the ionic state of the surrounding molecular components. The present study also implies that even a trace amount of phosphorylated tau molecules could strongly initiate fibrillogenesis in neurons.

This study must be extended to several directions. First, amyloid formation of proteins including tau is finely controlled by interaction with the surrounding media (*44*−*46*). The phosphorylation of tau might alter these interactions with environments. A close investigation on this point is essential for getting deeper insights into events in biological conditions. It would also be important to test whether phosphorylation of serine and threonine residues of tau similarly influences the amyloid-forming propensity of tau.

SUPPORTING INFORMATION AVAILABLE

TEM images of the fibrils generated by PHF6CF, PHF6OH, and PHF6E in solutions without HFIP; the synthesis method and the aggregation kinetic traces for PHF6A and PHF6S; the kinetic traces without normalization for PHF6CF, PHF6OH, PHF6E, PHF6EpY, and PHF6EAmF; energetic values obtained from simulation analysis of hypothetical fibril structures of PHF6 and its derivatives. This material is available free of charge via the Internet at http://pubs.acs.org.

REFERENCES

1. Gazit, E. (2002) A possible role for pi-stacking in the self-assembly of amyloid fibrils. *FASEB J. 16*, 77–83.
2. Goux, W. J., Kopplin, L., Nguyen, A. D., Leak, K., Rutkofsky, M., Shanmuganandam, V. D., Sharma, D., Inouye, H., and Kirschner, D. A. (2004) The formation of straight and twisted filaments from short tau peptides. *J. Biol. Chem. 279*, 26868–26875.
3. Azriel, R., and Gazit, E. (2001) Analysis of the minimal amyloid-forming fragment of the islet amyloid polypeptide. An experimental support for the key role of the phenylalanine residue in amyloid formation. *J. Biol. Chem. 276*, 34156–34161.
4. Petkova, A. T., Ishii, Y., Balbach, J. J., Antzutkin, O. N., Leapman, R. D., Delaglio, F., and Tycko, R. (2002) A structural model for Alzheimer's beta -amyloid fibrils based on experimental constraints from solid state NMR. *Proc. Natl. Acad. Sci. U.S.A. 99*, 16742–16747.
5. Gong, C.-X., Liu, F., Grundke-Iqbal, I., and Iqbal, K. (2005) Post-translational modifications of tau protein in Alzheimer's disease. *J. Neural. Transm. 112*, 813–838.
6. Nagano, S., Huang, X., Moir, R. D., Payton, S. M., Tanzi, R. E., and Bush, A. I. (2004) Peroxidase activity of cyclooxygenase-2 (COX-2) cross-links beta-amyloid (Abeta) and generates Abeta-COX-2 hetero-oligomers that are increased in Alzheimer's disease. *J. Biol. Chem. 279*, 14673–14678.
7. Terwel, D., Muyllaert, D., Dewachter, I., Borghgraef, P., Croes, S., Devijver, H., and Van Leuven, F. (2008) Amyloid activates GSK-3beta to aggravate neuronal tauopathy in bigenic mice. *Am. J. Pathol. 172*, 786–798.
8. Yankner, B. A., Duffy, L. K., and Kirschner, D. A. (1990) Neurotrophic and neurotoxic effects of amyloid beta protein: reversal by tachykinin neuropeptide. *Science 250*, 279–282.
9. Fernandez-Escamilla, A. M., Rousseau, F., Schymkowitz, J., and Serrano, L. (2004) Prediction of sequence-dependent and mutational effects on the aggregation of peptides and proteins. *Nat. Biotechnol. 22*, 1302–1306.
10. Li, W., and Lee, V. M. (2006) Characterization of two VQIXXK motifs for tau fibrillization in vitro. *Biochemistry 45*, 15692–15701.
11. Thompson, M. J., Sievers, S. A., Karanicolas, J., Ivanova, M. I., Baker, D., and Eisenberg, D. (2006) The 3D profile method for identifying fibril-forming segments of proteins. *Proc. Natl. Acad. Sci. U.S.A. 103*, 4074–4078.
12. Nelson, R., Sawaya, M. R., Balbirnie, M., Madsen, A. O., Riekel, C., Grothe, R., and Eisenberg, D. (2005) Structure of the cross-beta spine of amyloid-like fibrils. *Nature 435*, 773–778.
13. Sawaya, M. R., Sambashivan, S., Nelson, R., Ivanova, M. I., Sievers, S. A., Apostol, M. I., Thompson, M. J., Balbirnie, M., Wiltzius, J. J. W., McFarlane, H. T., Madsen, A. Ø., Riekel, C., and Eisenberg, D. (2007) Atomic structures of amyloid cross-beta spines reveal varied steric zippers. *Nature 447*, 453–457.
14. Lee, H. G., Perry, G., Moreira, P. I., Garrett, M. R., Liu, Q., Zhu, X., Takeda, A., Nunomura, A., and Smith, M. A. (2005) Tau phosphorylation in Alzheimer's disease: pathogen or protector. *Trends Mol. Med. 11*, 164–169.
15. Avila, J. (2006) Tau phosphorylation and aggregation in Alzheimer's disease pathology. *FEBS Lett. 580*, 2922–2927.
16. Johnson, G. V. (2006) Tau phosphorylation and proteolysis: insights and perspectives. *J. Alzheimers Dis. 9*, 243–250.
17. Hooper, C., Killick, R., and Lovestone, S. (2008) The GSK3 hypothesis of Alzheimer's disease. *J. Neurochem. 104*, 1433–1439.
18. Grundke-Iqbal, I., Iqbal, K., Tung, Y.-C., Quinlan, M., Wisniewski, H. M., and Binder, L. (1986) Abnormal phosphorylation of the microtubule-associated protein tau in Alzheimer cytoskeletal pathology. *Proc. Natl. Acad. Sci. U.S.A. 83*, 4913–4917.
19. Lee, V. M.-Y., Balin, B. J., Jr., and Trojanowski, J. Q. (1991) A68: a major subunit of paired helical filaments and derivatized forms of normal Tau. *Science 251*, 675–678.
20. Goedert, M., Spillantini, M. G., Cairns, N. J., and Crowther, R. A. (1992) Tau proteins of Alzheimer paired helical filaments: abnormal phosphorylation of all six brain isoforms. *Neuron 8*, 159–168.
21. Alonso, A., Zaidi, T., Novak, M., Grundke-Iqbal, I., and Iqbal, K. (2001) Hyperphosphorylation induces self-assembly of tau into tangles of paired helical filaments/straight filaments. *Proc. Natl. Acad. Sci. U.S.A. 98*, 6923–6928.
22. Schneider, A., Biernat, J., von Bergen, M., Mandelkow, E., and Mandelkow, E. M. (1999) Phosphorylation that detaches tau protein from microtubules (Ser262, Ser214) also protects it against aggregation into Alzheimer paired helical filaments. *Biochemistry 38*, 3549–3558.
23. Vega, I. E., Cui, L., Propst, J. A., Hutton, M. L., Lee, G., and Yen, S.-H. (2005) Phosphorylation that detaches tau protein from microtubules (Ser262, Ser214) also protects it against aggregation into Alzheimer paired helical filaments. *Brain Res. Mol. Brain Res. 138*, 135–144.
24. Derkinderen, P., Scales, T. M. E., Hanger, D. P., Leung, K.-Y., Byers, H. L., Ward, M. A., Lenz, C., Price, C., Bird, I. N., Perera, T., Kellie, S., Williamson, R., Noble, W., Van Etten, R. A., Leroy, K., Brion, J.-P., Reynolds, C. H., and Anderton, B. H. (2005) Tyrosine 394 is phosphorylated in Alzheimer's paired helical filament tau and in fetal tau with c-Abl as the candidate tyrosine kinase. *J. Neurosci. 25*, 6584–6593.
25. Lee, G., Thangavel, R., Sharma, V. M., Litersky, J. M., Bhaskar, K., Fang, S. M., Do, L. M., readis, A., Hoesen, G. V., and Ksiezak-Reding, H. (2004) Phosphorylation of tau by fyn: implications for Alzheimer's disease. *J. Neurosci. 24*, 2304–2312.
26. Wischik, C. M., Novak, M., Thøgersen, H. C., Edwards, P. C., Runswick, M. J., Jakes, R., Walker, J. E., Milstein, C., Roth, M., and Klug, A. (1988) Isolation of a fragment of tau derived from the core of the paired helical filament of Alzheimer disease. *Proc. Natl. Acad. Sci. U.S.A. 85*, 4506–4510.
27. Wille, H., Drewes, G., Biernat, J., Mandelkow, E. M., and Mandelkow, E. (1992) Alzheimer-like paired helical filaments and antiparallel dimers formed from microtubule-associated protein tau in vitro. *J. Cell Biol. 118*, 573–584.
28. Konno, T., Oiki, S., Hasegawa, K., and Naiki, H. (2004) Anionic contribution for fibrous maturation of protofibrillar assemblies of the human tau repeat domain in a fluoroalcohol solution. *Biochemistry 43*, 13613–13620.
29. von Bergen, M., Friedhoff, P., Biernat, J., Heberle, J., Mandelkow, E.-M., and Mandelkow, E. (2000) Assembly of tau protein into Alzheimer paired helical filaments depends on a local sequence motif ((306)VQIVYK(311)) forming beta structure. *Proc. Natl. Acad. Sci. U.S.A. 97*, 5129–5134.
30. Rojas Quijano, F. A., Morrow, D., Wise, B. M., Brancia, F. L., and Goux, W. J. (2006) Prediction of nucleating sequences from amyloidgenic propensities of tau-related peptides. *Biochemistry 45*, 4638–4652.
31. Hirata, A., Sugimoto, K., Konno, T., and Morii, T. (2007) Amyloid-forming propensity of the hydrophobic non-natural amino acid on the fibril-forming core peptide of human tau. *Bioorg. Med. Chem. Lett. 17*, 2971–2974.
32. Edelhoch, H. (1967) Spectroscopic determination of tryptophan and tyrosine in proteins. *Biochemistry 6*, 1948–1954.
33. Habeeb, A. F. S. A. (1966) Determination of free amino groups in proteins by trinitrobenzenesulfonic acid. *Anal. Biochem. 14*, 328–336.
34. LeVine, H. (1993) Thioflavine T interaction with synthetic Alzheimer's disease beta-amyloid peptides: detection of amyloid aggregation in solution. *Protein Sci. 2*, 404–410.
35. Ding, H.-Q., Naoki, K., and Goddard III, W. A. (1992) Atomic level simulations on a million particles: The cell multipole method for Coulomb and London nonbond interactions. *J. Chem. Phys. 97*, 4309–4315.
36. Jarrett, J. T., and Lansbury, P. T., Jr. (1993) Seeding "one-dimensional crystallization" of amyloid: a pathogenic mechanism in Alzheimer's disease and scrapie? *Cell 73*, 1055–1058.
37. Lomakin, A., Chung, D. S., Benedek, G. B., Kirschner, D. A., and Teplow, D. B. (1996) On the nucleation and growth of amyloid beta-protein fibrils: detection of nuclei and quantitation of rate constants. *Proc. Natl. Acad. Sci. U.S.A. 93*, 1125–1129.
38. Haris, P. I., and Chapman, D. (1995) The conformational analysis of peptides using Fourier transform IR spectroscopy. *Biopolymers 37*, 251–263.

39. Crowther, R. A. (1991) Straight and paired helical filaments in Alzheimer disease have a common structural unit. *Proc. Natl. Acad. Sci. U.S.A. 88*, 2288–2292.
40. Barghorn, S., Davies, P., and Mandelkow, E. (2004) Tau paired helical filaments from Alzheimer's disease brain and assembled in vitro are based on beta-structure in the core domain. *Biochemistry 43*, 1694–1703.
41. Goedert, M., Jakes, R., Spillantini, M. G., Hasegawa, M., Smith, M. J., and Crowther, R. A. (1996) Assembly of microtubule-associated protein tau into Alzheimer-like filaments induced by sulphated glycosaminoglycans. *Nature 383*, 550–553.
42. King, M. E., Gamblin, T. C., Kuret, J., and Binder, L. I. (2000) Differential assembly of human tau isoforms in the presence of arachidonic acid. *J. Neurochem. 74*, 1749–1757.
43. Chirita, C. N., Necula, M., and Kuret, J. (2003) Anionic micelles and vesicles induce tau fibrillization in vitro. *J. Biol. Chem. 278*, 25644–25650.
44. Friedhoff, P., von Bergen, M., Mandelkow, E. M., and Mandelkow, E. (2000) Structure of tau protein and assembly into paired helical filaments. *Biochim. Biophys. Acta 1502*, 122–132.
45. Gamblin, T. C., Berry, R. W., and Binder, L. I. (2003) Modeling tau polymerization in vitro: a review and synthesis. *Biochemistry 42*, 15009–15017.
46. Konno, T., Oiki, S., and Morii, T. (2007) Synergistic action of polyanionic and non-polar cofactors in fibrillation of human islet amyloid polypeptide. *FEBS Lett. 581*, 1635–1638.

BI8010994